Enhancing the Output Performance of Triboelectric Nanogenerator via Grating-Electrode-Enabled Surface Plasmon Excitation

Lingxiao Gao, Xin Chen, Shan Lu, Hong Zhou, Weibo Xie, Junfei Chen, Mengke Qi, Hua Yu, Xiaojing Mu,* Zhong Lin Wang,* and Ya Yang*

The surface charge density and the output impedance of triboelectric nano-generators (TENGs) are two critical factors for TENGs to speed up their commercialization, so it is important to explore unique methods to reduce the output impedance and increase the surface charge density. Here, an approach is demonstrated to effectively boost the output performance of TENG while reducing the output impedance of TENGs by utilizing grating-electrode-enabled surface plasmon excitation. A sustainable and enhanced output performance of about 40 µA (short-circuit current) and 350 V (peak-to-peak voltage at a resistance of 10 MΩ) is produced via grating-coupled surface plasmon resonance on the TENG with the aluminum grating electrode in the line density of 600 lines mm^{-1}, and it delivers a peak output power of 3.6 mW under a loading resistance of 1 MΩ, giving over 4.5-fold enhancement in output power and a 75% reduction in the output impedance. Finally a self-powered ultrasonic ranging system is utilized to verify the capability of the TENG in powering portable electrics.

1. Introduction

As energy crisis has become a serious problem in the world, intensive research efforts have been devoted to explore new energy resources. Triboelectric nanogenerators (TENGs) as a new energy harvesting technology with unprecedented output performance and relatively low cost have been demonstrated as a leading candidate for numerous applications in energy harvesting and self-powered sensing.[1–5] It plays an increasingly important role with the fast depletion of fossil fuels. As an energy harvester, the output characteristic of the TENGs is the key consideration, which involves two main aspects: the surface charge density[6–8] and the output impedance.[9,10] Till now, studies have been conducted on the improvement of the surface charge density, such as surface functionalization techniques including micropatterning surface,[11–20] plasma treatment,[21] or adding chemical functional groups.[22–25] Especially substantial researches on the TENGs have concentrated on making triboelectric layers into both micro- and nanoscale to achieve increased surface areas and roughness.[26] However, there is a lack of effective means to reduce the output impedance.

Plasmonic energy conversion proposed as a high efficiency scheme to electron–hole separation opens up a wide range of applications in the field of subwavelength optics,[27] data storage,[28] nonlinear optics,[29] solar cells,[30] and

Dr. L. X. Gao, Dr. X. Chen, Dr. S. Lu, Dr. H. Zhou, J. F. Chen,
Dr. M. K. Qi, Prof. H. Yu, Prof. X. J. Mu
Key Laboratory of Optoelectronic Technology
& Systems Ministry of Education
International R & D Center of Micro-Nano Systems and
New Materials Technology
Chongqing University
Chongqing 400044, P. R. China
E-mail: mxjacj@cqu.edu.cn
Dr. L. X. Gao, Dr. X. Chen, Dr. H. Zhou, Prof. Z. L. Wang, Prof. Y. Yang
CAS Center for Excellence in Nanoscience
Beijing Key Laboratory of Micro-nano Energy and Sensor
Beijing Institute of Nanoenergy and Nanosystems
Chinese Academy of Sciences
Beijing 100083, P. R. China
E-mail: yayang@binn.cas.cn

Dr. W. B. Xie
State Key Laboratory of Mechanical Transmissions
Chongqing University
Chongqing 400044, P. R. China
Prof. Z. L. Wang
School of Material Science and Engineering
Georgia Institute of Technology
Atlanta, GA 30332-0245, USA
E-mail: zhong.wang@mse.gatech.edu
Prof. Z. L. Wang, Prof. Y. Yang
School of Nanoscience and Technology
University of Chinese Academy of Sciences
Beijing 100049, P. R. China
Prof. Y. Yang
Center on Nanoenergy Research
School of Physical Science and Technology
Guangxi University
Nanning, Guangxi 530004, P. R. China

ADVANCED
SCIENCE NEWS
www.advancedsciencenews.com

ADVANCED
ENERGY
MATERIALS
www.advenergymat.de

biophotonics.[31] Several investigations have demonstrated that surface plasmons can decay into hot electron–hole pairs,[32,33] which can significantly change the conductivity.[34] Therefore, it can be assumed that the surface plasmon resonance can change the output impedance of the TENGs on the basis of affecting their output performance.

Here, we demonstrated an approach to effectively enhance the output performance of TENGs via grating-electrode-enabled surface plasmon excitation. It was proposed that the presence of hot electron–hole pairs decayed from the surface plasmon resonance could effectively enhance the output of TENGs while reduce their output impedances. Firstly, we magically found that the grating-coupled surface plasmon resonance on the digital versatile disks (DVDs) can significantly enhance the output performance of the TENG. By comparing several different materials, a sustainable and enhanced output performance of 110 μA (short-circuit current) and 410 V (peak-to-peak voltage at a resistance of 50 MΩ) were produced on the DVD, and it delivered a peak output power of 14.45 mW under a loading resistance of 2 MΩ, giving over five-fold enhancement in output power. The reduction of the output impedance by 50% was also achieved. This is because the hot electron–hole pairs decayed from surface plasmon resonance could act as negative charge traps to enhance the triboelectric layer's capability of capturing charges during contact electrification. To further verify this effect, a series of TENGs with different line densities (0, 100, 300, 600 lines mm^{-1}) on the bottom electrode were developed, and the output performance of the TENG with the line density of 600 lines mm^{-1} on the bottom electrode exhibits a remarkable improvement by about 4.5 times while its output impedance is reduced more than four times. Furthermore, through light and dark treatment experiments, it was further verified that the enhancement is not due to the instantaneous effect of surface plasmon resonance, but the hot hole-pairs effect. A systematical effect of the light intensity and wavelength on the output of TENG was also acquired. Our findings may also give new insights into the improvement of the output characteristics of TENGs and accelerate their commercialization and applications.

2. Results and Discussion

2.1. The Theoretical Model of the Grating-Electrode-Enabled Surface Plasmon Excitation Enhanced TENGs

The excitation of surface plasmon at a metal-dielectric interface requires that the wave vector of incident light (κ_x) matches that of the surface plasmon (κ_{sp}). The real part of the κ_{sp} can be described as the following formula[31]

$$\kappa'_{sp} = \frac{2\pi}{\lambda_0} \sqrt{\frac{\varepsilon'_M \varepsilon_D}{\varepsilon'_M + \varepsilon_D}} \qquad (1)$$

where λ_0 is the wavelength of incident light while ε_D and ε_M denote the dielectric constants of the dielectric layer and metal layer respectively. Since the momentum of incident light in air is lower than that of the surface plasmon, in other words, the wave vectors of them cannot match in air, a coupling method is needed. Metal diffraction grating is one of the most used methods to excite surface plasmon. Through the grating

coupling, the surface component of the κ_x can be increased (or decreased) as displayed in Figure S1 (Supporting Information). If this increase (or decrease) matches κ_{sp}, it will excite surface plasmon and the relationship can be expressed as

$$\kappa'_{sp} = \frac{2\pi}{\lambda_0} \sqrt{\frac{\varepsilon'_M \varepsilon_D}{\varepsilon'_M + \varepsilon_D}} = \frac{2\pi}{\lambda_0} \sqrt{\varepsilon_D} \sin\theta_0 + m \frac{2\pi}{\Lambda} = \kappa'_x \qquad (2)$$

where θ_0 is the angle of incidence while m and Λ indicate the diffracted order and the grating period, respectively.

It has been demonstrated that the surface plasmons excited in the metal diffraction gratings can decay on a femtosecond timescale, producing electron–hole pairs,[35] a unit as illustrated in **Figure 1**a. Based on this theory, the basic theoretical model of the grating-coupled surface plasma-enhanced TENG was constructed. The schematic diagrams of the electricity generation process of the TENG with grating-coupled surface plasmon resonance are displayed in Figure 1b, where the TENG has a double-layer structure. The first layer is a piece of metal foil 1 attached onto poly methyl methacrylatemethacrylic acid (PMMA) as one triboelectric layer. The second layer is another piece of metal foil 2 with a periodic grating structure attached onto another PMMA, and a piece of dielectric film which is much more triboelectrically negative than the metal foil 1 was applied to metal foil 2 with grating structure as another triboelectric layer.[36] The surface plasmon resonance can be excited on the surface of metal foil 2 with grating structure under a solar simulator, and it will decay into hot electron–hole pairs in the time scale of 1–100 fs,[32,33] which will distribute at the interface between the dielectric film and metal foil 2 (Figure 1b (I)). Under an external force, the metal foil 1 and dielectric film would be brought into full contact with each other. Because dielectric film is much more triboelectrically negative than metal foil 1, so electrons would flow from metal foil 1 into dielectric film, resulting in an accumulation of net opposite charges on the dielectric film and the metal foil 1 (Figure 1b (II)). When an external force was withdrawn, the metal foil 1 and dielectric film moved apart and the electrons would flow from the metal foil 2 to the metal foil 1, resulting in a forward current signal for the TENG (Figure 1b (III)). Since the surfaces of the dielectric film and metal foil 2 accumulate net opposite charges, it was going to create an electric field from the metal foil 2 to the dielectric film, resulting in the vertical arrangement of some hot electron–hole pairs. Then the first layer was completely back to its original position. The electric field from the metal foil 2 to the dielectric film reached its maximum, resulting in the vertical arrangement of all of hot electron–hole pairs (Figure 1b (IV)). And they would act as negative charge traps to enhance the dielectric film's capability of capturing charges during contact electrification.[37] When the force was reapplied, the electrons flowed from the metal foil 1 to the metal foil 2, forming a reverse current (Figure 1b (V)). It is important to note that in this process (III–IV–V) there were only triboelectric charge pairs without surface plasmon effect. When the metal foil 1 and dielectric film were brought into full contact with each other again, the electric field would disappear. But the vertical hot electron–hole pairs would not fully diminish due to dielectric hysteresis, resulting in the accumulation of more net opposite charges on the metal foil 1 and the dielectric film
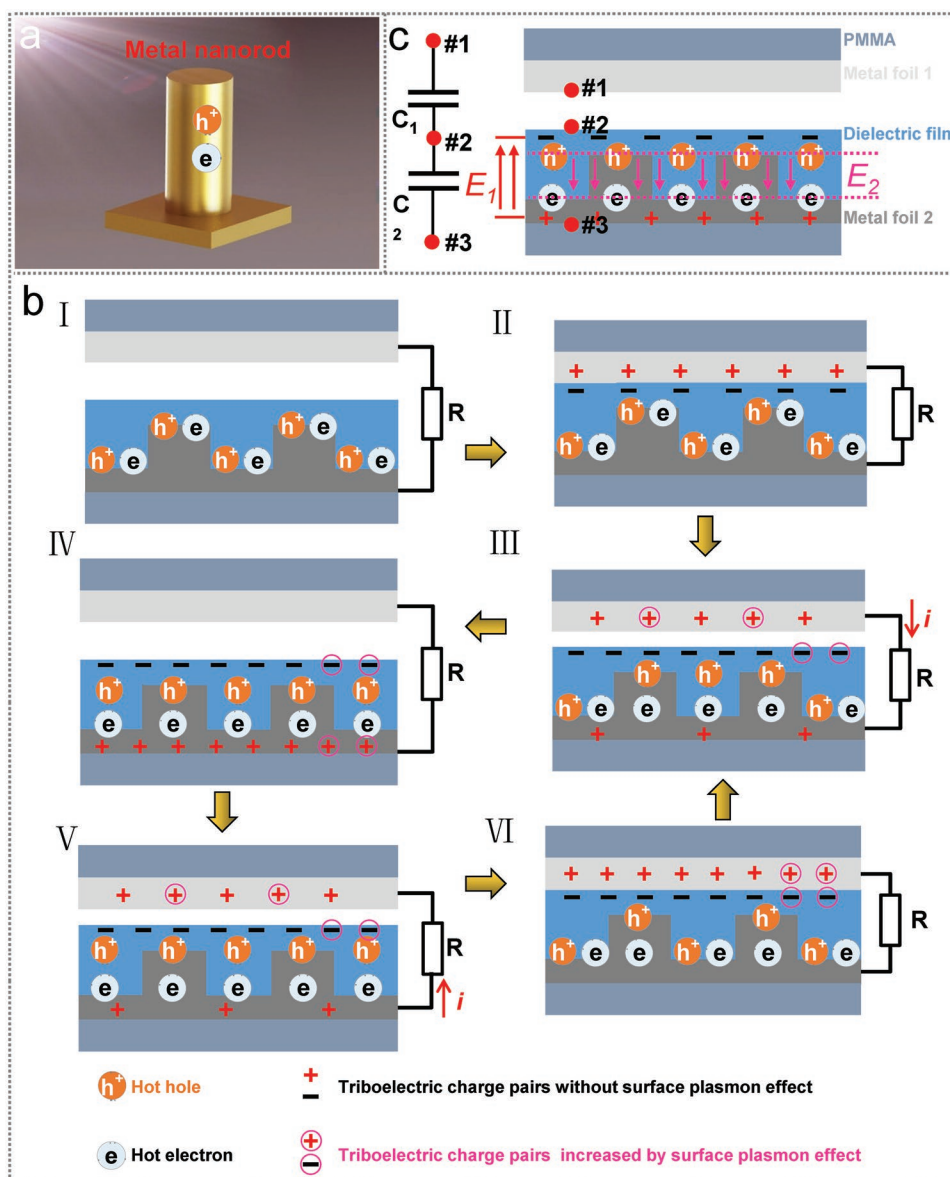
**ADVANCED
SCIENCE NEWS**

www.advancedsciencenews.com

**ADVANCED
ENERGY
MATERIALS**

www.advenergymat.de

Figure 1. Theoretical model of the grating-coupled surface-plasma-enhanced TENGs. a) The generation of hot electron–hole pairs. b) Schematic diagrams of the electricity generation process of the TENG with grating-coupled surface plasmon resonance. c) Theoretical models of reverse electric field established by hot electron–hole pairs.

(Figure 1b (VI)). It starts with triboelectric charge pairs increased by surface plasmon effect in this state (VI), and keeps going to the next cycle (VI–III–IV–V). In other words, the electric field generated by triboelectrification will cause the hot electron–hole pairs decayed from the surface plasmon resonance to align vertically, while the latter can enhance the former in subsequent contact electrification processes until an equilibrium is reached. During the periodical contact–separation motion, a periodic alternating enhanced current (AC) will be generated.

Theoretical models for conductor-to-dielectric contact-mode TENG whose equivalent circuit is a series of two capacitors (C_1 and C_2) as depicted in Figure 1c. When the equilibrium is reached, an electric field (E_2) will be established by the hot electron–hole pairs between the dielectric film and metal foil 2,

and the direction of this electric field will be opposite to that generated by triboelectrification (E_1), as diagramed in Figure 1c. The total field strength in the capacitor (C_2) is weakened, resulting in a reduced voltage (U) between the dielectric film and metal foil 2. Assuming that the electric quantity (Q) of the capacitor (C_2) is constant, the capacitor (C_2) will increase, which can be obtained from formula (3)

$$C_2 = \frac{Q}{U} \tag{3}$$

The equivalent capacitance (C) of the TENG is

$$C = \frac{C_1 * C_2}{C_1 + C_2} \tag{4}$$

So an increase in C_2 will lead to an increase in C. The output impedance of the capacitor is

$$Z = \frac{1}{j\omega C} \tag{5}$$

Hence, a reduction of the output impedance will be obtained.

2.2. Performances of the TENGs with Grating Electrode Based on CDs and DVDs

Gratings on the metal interface have attracted significant interests for exciting plasma effect. However, to obtain such patterns, very expensive fabrication processes are typically needed to create the pre-designed nanostructures. Fortunately, it has been demonstrated that surface plasmon effects can be excited in the visible light range via inexpensive and disposable plastic gratings on commercially available compact disks (CDs) and DVDs.[38] Therefore, we first used inexpensive CDs and DVDs for principle experimental verification.

Based on the above theoretical analysis, finite-different time-domain simulations were performed to study grating-coupled surface plasmon resonance on the DVDs, as displayed in Figure S2 (Supporting Information). First, the DVDs with and without the metallic bump were simulated respectively. Figure S2a$_1$,a$_2$ (Supporting Information) shows the electric-field intensity maps of far field and near field of DVDs without the metallic bump, while Figure S2b$_1$,b$_2$ (Supporting Information) shows the electric-field intensity maps of far field and near field of DVDs with the metallic bump. It shows a local electric field was enhanced on the DVDs with the metallic bump. Second, the DVDs with (Figure S2c$_2$, Supporting Information) and without (Figure S2c$_1$, Supporting Information) grating structure had been simulated under the condition of incident angle at 20° and p-polarized light at 550 nm. It clearly reveals a strongly enhanced electric field at the interface of the dye and Al grating.

Inexpensive CDs and DVDs were employed for principle experimental verification. As sketched in **Figure 2**a, the TENG has a double-layer structure. The first layer is a piece of thin copper foil attached onto a piece of PMMA. The second layer is a piece of compact disks. The CDs used in this work consisted of sequential layers of polycarbonate (PC), dye, Al, protective lacquer, silk screen layers illustrated in Figure 2a, and the cross-sectional scanning electron microscopy (SEM) image of it is shown in Figure 2b. Aluminum foil with periodic grating structure was employed as a metal layer that excites the surface plasmon effect, which is depicted in Figure 2c. As illustrated in atomic force microscopy (AFM) image, the grating structure has a periodicity of ≈1.6 µm and a depth of ≈110 nm. The top layer (PC) of the CDs was employed as one triboelectric layer. DVDs have a similar disk structure to CDs, except that the thickness of disc (0.6 mm) is half of that of CDs' (1.2 mm) and the periodicity is 0.74 µm. In other words, a piece of DVD consists of two substrates, each with a thickness of 0.6 mm.

It can be known from the above analysis, the surface plasmon resonance can improve the output performance of the TENGs on the basis of reducing its output impedance. Inexpensive CDs or DVDs was employed as one triboelectric layer

for principle experimental verification as revealed in Figure 2. The output performance of the TENG was carried out under a linear motor. The aluminum foil with a grating structure on the lower layer of the CDs was scraped off gently, and a piece of aluminum foil without a grating structure was affixed on the CDs as the contrast device. As revealed in Figure 2d, the outputs of the TENG with Al-grating structure are definitely higher than those without. A sustainable output of 410 V (peak-to-peak voltage at a resistance of 50 MΩ), 110 µA (short-circuit current), 250 nC was produced via grating-coupled surface plasmon resonance on the DVDs, while 300 V at a resistance of 50 MΩ, 100 µA short-circuit current, 210 nC and 200 V at a resistance of 50 MΩ, 25 µA short-circuit current, 60 nC for the CDs and the CDs without metal grating structure, respectively. Another interesting phenomenon is that the outputs of the TENG based on DVDs are higher than those based on CDs. In other words, the surface plasmon effect was better coupled on the DVDs. It is associated with two reasons. One is the thickness of the DVDs (0.6 mm) is half of that of the CDs (1.2 mm), in other words, the metal grating structure on the DVDs is half as close to the triboelectric layer (PC) as it is to the CDs. Another is the line density of DVDs is higher than that of CDs, which will be verified in the later experiment.

Based on aforementioned testing results, the output powers of the TENGs based on CDs without a metal grating structure, the CDs, and DVDs were also measured with external loads from 0.01 to 10 MΩ, as illustrated in Figure 2e. The top curve is the instantaneous power point of the TENG based on the CDs without the metal grating structure, and it can deliver a peak output power of 2.645 mW under a loading resistance of 5 MΩ. The middle and bottom curves are the instantaneous power points of the TENGs based on the CDs and DVDs. The peak power of the TENG based on the CDs is 11.25 mW at a resistance of 2 MΩ, while 14.45 mW is for the TENG based on the DVDs at a resistance of 2 MΩ. It shows definitely an enhancement in output power and a reduction in the output impedance were achieved via grating-coupled surface plasmon resonance. Especially, the TENG based on the DVDs gave over fivefold enhancement in output power and 50% reduction of the output impedance compared with the TENG without grating-coupled surface plasmon resonance. Meanwhile, the charging rate of the TENG based on the DVDs has been significantly improved compared with the TENG without grating-coupled surface plasmon resonance, as presented in Figure S3 (Supporting Information).

To further verify the enhancement of grating-coupled surface plasmon resonance on the CDs and DVDs, several different transparent materials (polyethylene (PE), polyethylene terephthalate (PET), polytetrafluoroethylene (PTFE)) were pasted on the PC layer of the DVDs and CDs respectively, which were employed as triboelectric layers. Figure S4a$_1$–a$_3$ (Supporting Information) shows the outputs of the TENGs with PE, while Figure S4b$_1$–b$_3$,c$_1$–c$_3$ (Supporting Information) shows the outputs of the TENGs with PET and PTFE, respectively. They also demonstrate that the output of the TENGs with metal grating structure is definitely higher than those without. However, their outputs are lower than those with pure DVDs. This is because the increase of the distance between the hot electron–hole pairs and triboelectric layer reduces the enhancement effect.
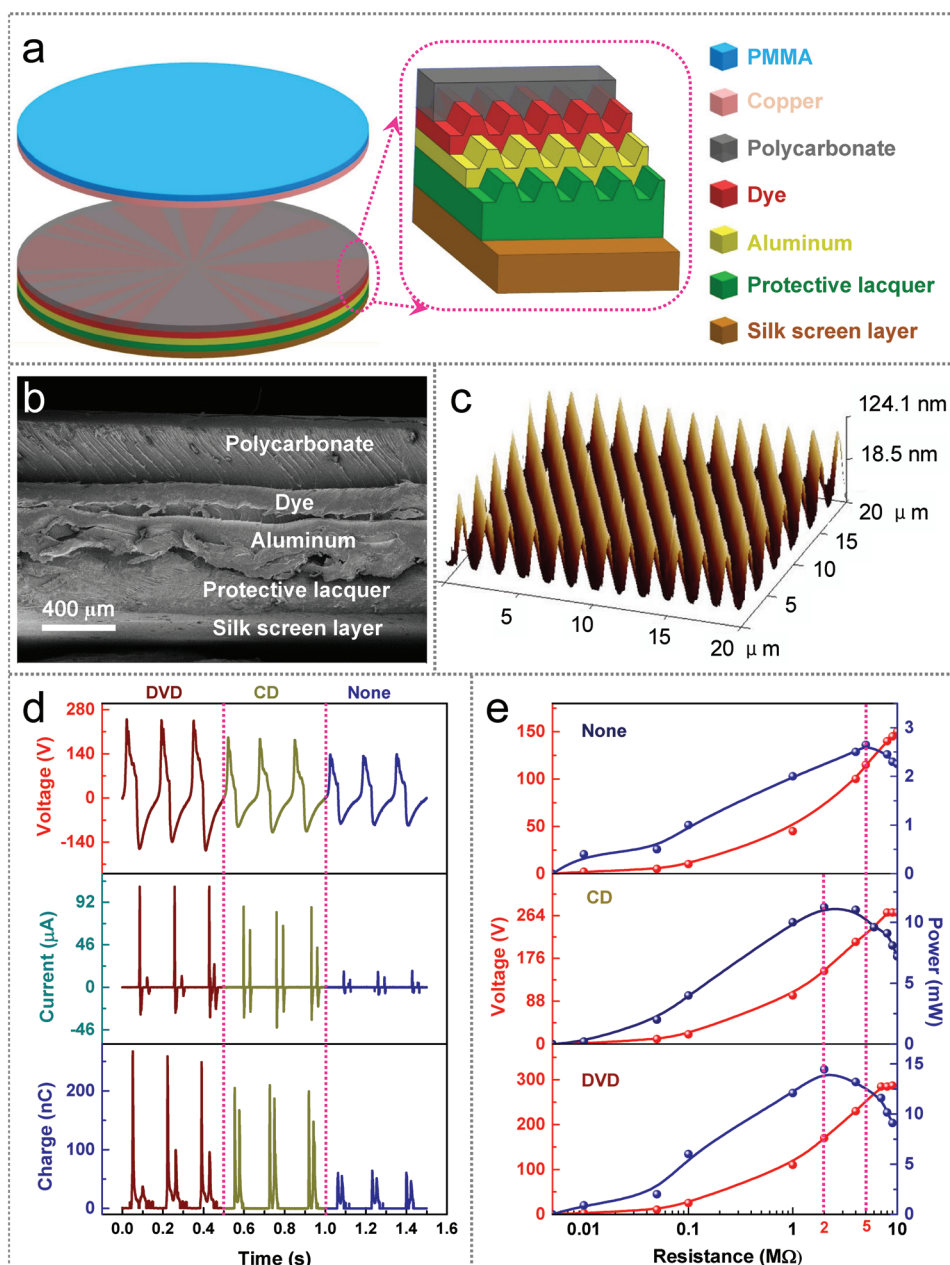
Figure 2. TENGs with grating electrode based on the CDs and DVDs. a) Schematic of the TENG with a double-layer structure based on the CDs. b) Cross-sectional scanning electron microscope (SEM) image of the CDs. c) AFM microscopy image showing details of raster structure on the aluminum foil. d) The output performance of the TENG based on the DVDs, CDs, and CDs without a metal grating structure. e) The instantaneous power points of the TENG based on the CDs without a metal grating structure, CDs, and DVDs.

2.3. Fabrication of TENG with Different Line Density Gratings and Electrical Outputs

The previous analysis shows that the outputs of the TENG based on the DVDs are higher than those based on CDs, and it is associated with the difference of their line densities. So four pieces of aluminum foil with different line densities (0, 100, 300, 600 lines mm^{-1}) were chosen for further verification experiment. **Figure 3**a$_1$–a$_4$ shows digital photographs of the aluminum foil in the line densities of 0, 100, 300, and

600 lines mm^{-1}. Figure 3b$_1$ displays the AFM microscopy image of the aluminum foil without a grating structure whose roughness is about 200 nm. Figure 3b$_2$ presents the AFM microscopy image of the aluminum foil with the line density of 100 lines mm^{-1}, and from the details we can see the grating structure has a periodicity of ≈10 µm and a depth of ≈367 nm. Figure 3b$_3$ shows the aluminum foil with the line density of 300 lines mm^{-1} has a periodicity of ≈3.3 µm and a depth of ≈483 nm. A periodicity of ≈1.6 µm and a depth of ≈640 nm for the aluminum foil with the line density of 600 lines mm^{-1} illustrated

**ADVANCED
SCIENCE NEWS**
www.advancedsciencenews.com
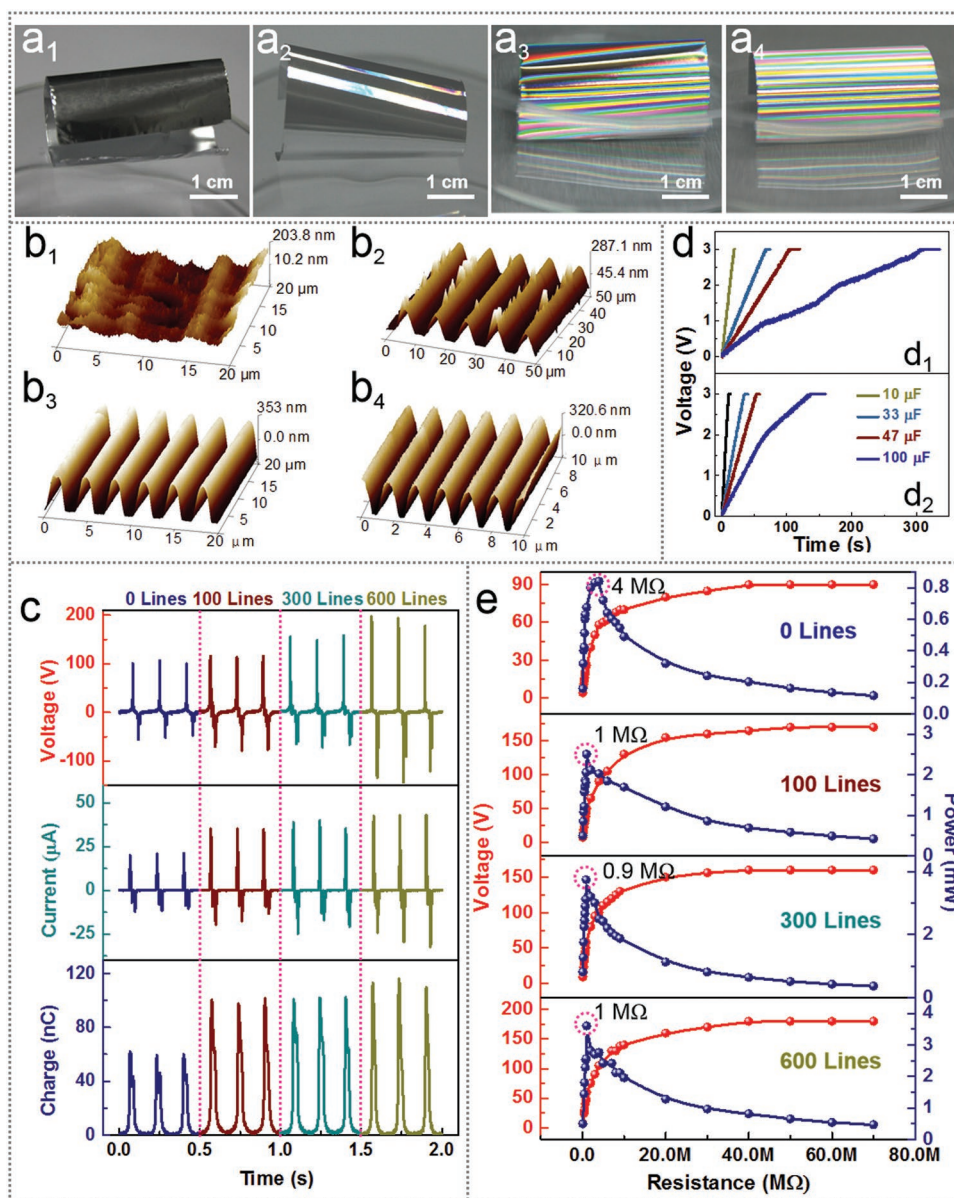
**ADVANCED
ENERGY
MATERIALS**
www.advenergymat.de

Figure 3. The TENG with the aluminum foil in different line densities. a_1–a_4) Digital photograph of the aluminum foil in different line densities. b_1–b_4) AFM microscopy image showing details of the aluminum foil in different line densities. c) The outputs of the TENG with the aluminum foil in different line densities. d) The charge times of the TENG with the aluminum foil in the line density of d_1) 0 and d_2) 600 lines mm^{-1}. e) The maximum power points of the TENG with the aluminum foil in different line densities.

in Figure 3b_4. A Spin coating technique was used to fabricate the polydimethylsiloxane (PDMS) film with aluminum foil in different line densities (0, 100, 300, 600 lines mm^{-1}). The fabrication process is shown in Figure S5 (Supporting Information) and for details, see Methods (Supporting Information).

The output performances of the TENG with the aluminum foil in different line densities were measured under a constant contact force from the linear motor. Figure 3c illustrates the outputs of the TENG with the aluminum foil in different line densities at a resistance of 10 MΩ. As revealed in Figure 3c, the voltages (at a resistance of 10 MΩ) of the TENG with the aluminum foil in different line densities are higher than those without, and with the increase of line density of aluminum foil,

the voltages rise likewise. The maximum value about 350 V (peak-to-peak voltage at a resistance of 10 MΩ) was achieved for the TENG with the aluminum foil in the line density of 600 lines mm^{-1} which was two times of that without. In current curves and charge curves, they indicate that the short-circuit currents and the transfer charges quantity follow a similar trend with the voltages, and a maximum value of 40 μA, 110 nC were also obtained for the TENG with the aluminum foil in the line density of 600 lines mm^{-1}. The charging capacities of the TENG with the aluminum foil in the line density of 0 and 600 lines mm^{-1} are described in Figure 3d. We can see that the charging rate of the TENG with the aluminum foil in the line density of 600 lines mm^{-1} has been significantly improved

compared with the TENG without grating surfaces and it can charge a 100 µF capacitor from 0 to 3 V in about 140 s. In order to further verify the power and impedance characteristics, the maximum power points of the TENG with the aluminum foil in the line densities of 0, 100, 300, 600 lines mm^{-1} were measured with external loads from 100 KΩ to 70 MΩ, as shown in Figure 3e. The output impedance is obviously reduced on the basis of increasing its power, and a peak output power of 3.6 mW was achieved under a loading resistance of 1 MΩ for the TENG with the aluminum foil in the line density of 600 lines mm^{-1}, giving over 4.5-fold enhancement in output power (0.8 mW) and 4.5-fold reduction in output impedance (4 MΩ) compared with the TENG with the aluminum foil in 0 lines mm^{-1}.

It is well known that the surface plasmon effect is a transient effect, which disappears with the disappearance of light. So the outputs of TENG with the aluminum foil in the line density of 600 lines mm^{-1} were measured with lights on and off, as depicted in Figure S6 (Supporting Information). Unfortunately, the instantaneous effect was not observed, and the outputs did not change with the lights on and off. In other words, it is not the instantaneous effect of surface plasma that increases the output performances of the TENG. While the hot electron–hole pair excited by surface plasmon effect dose not disappear immediately due to dielectric hysteresis. Therefore, in order to further verify the enhancement effect of hot electron–hole pair which we mentioned above, two pieces of TENG with the aluminum foil in 600 lines mm^{-1} were chosen for comparison. One was placed in light for 4 h while the other one in darkness for 4 h. The outputs of the TENGs which were placed in darkness are depicted in **Figure 4**a, and it can be clearly seen that the outputs had decreased significantly. Later, we placed it in the light for another hour and measured its outputs. Its outputs were restored to the original as illustrated in Figure 4a. It well verifies our theory of boosting the output performance of triboelectric nanogenerator via hot electron–hole pairs excited by grating-coupled surface plasmon resonance. In other words, hot electron–hole pairs had fully diminished after 4 h in darkness. The outputs of the TENG which was placed in light for 4 h had not improved (Figure 4b), and it is because the number of hot electron–hole pairs had reached saturation in the original ray.

An AM 1.5G solar simulator was employed as the excitation for surface plasmon as depicted in Figure 4c. The solar simulator was calibrated by a silicon reference cell to obtain a light intensity of 100 mW cm^{-2} as 1.0 times of the sunlight. Experiments of different light intensity (0 times, 0.2 times, 0.6 times, 0.8 times, 1.0 times of the sunlight) indicate that the output of the TENG with grating-electrode increases with the increase of light intensity (Figure 4d). The TENG with grating-electrode was illuminated for 30 min at each light intensity. As is known to all, when surface plasmon effect occurs, a sharp resonance dip will be observed in the reflectance of p-polarized light. The reflectivity curve of the grating-electrode in 600 lines mm^{-1} was calculated with the plane electrode as reference standard is shown in Figure 4e, and when the angle of incidence is 38 degrees, a sharp dip peak is clearly observed in 660.5 nm under illumination of p-polarized light (p-pol). At the same time, the output of TENG with grating-electrode in 600 lines mm^{-1} was

measured under 200–400 nm and 400–700 nm, and it demonstrates that the surface plasmon effects were excited in the visible light range (Figure 4f).

2.4. Power-Supplying System of the Ultrasonic Ranging System

Some experiments had been finished to demonstrate the capability of the TENG with the aluminum foil in the line density of 600 lines mm^{-1} to harvest mechanical energy. Figure S7a (Supporting Information) displays that the output of the TENG with the aluminum foil in the line density of 600 lines mm^{-1} remains almost constant after continuous operation for about 1000 cycles. A temperature sensor was driven by the TENG through connecting a rectified circuit and a capacitor of 10 µF in Figure S7b and Video S1 (Supporting Information). Then a self-powered ultrasonic ranging system was built to verify the capability of the TENG with the aluminum foil in the line density of 600 lines mm^{-1} in powering portable electrics, as presented in **Figure 5**a. Duo to the output of the TENG is alternating current, a rectified circuit and a 2000 µF were chosen to convert it to a direct current. Because the supply voltage of the ultrasonic ranging system is about 3 V, a buck-boost DC–DC circuit was used to achieve voltage matching. Finally, the data was displayed in real time in the monitoring system on a computer. Figure 5b displays the 2000 µF capacitor was charged from 0 to 5 V in about 30 min. Then turned on the ultrasonic ranging system and monitored voltages of capacitor (V1) and buck-boost DC-DC circuit (V2) demonstrated in Figure 5c. When the transceiver cycle of the ultrasonic ranging system was set to 2s, the stored power in the 2000 µF could support its operation for 16 cycles. Figure 5c displays when the output voltage (V1) of the capacitor was lower than 0.8 V, the voltage stabilizing effect of the buck-boost DC-DC circuit failed, and when the output voltage (V2) of the buck-boost DC–DC circuit was lower than 1.6 V, it could not support the ultrasonic ranging system. Figure 5d$_1$–d$_2$ shows the partial enlargements of V1 and V2 and it demonstrates the voltage drops of V1 and V2 when the ultrasonic ranging system sends and receives data. Figure 5e–f and Video S2 (Supporting Information) demonstrate an ultrasonic ranging system powered by the TENG with the aluminum foil in the line density of 600 lines mm^{-1}.

3. Conclusion

In summary, we have demonstrated an approach to effectively enhance the output performance of triboelectric nanogenerator via grating-electrode-enabled surface plasmon excitation. In addition, it has been proved theoretically and experimentally that the hot electron–hole pairs decayed from the surface plasmon resonance could effectively enhance the output of the TENG while reduce its output impedance. First, the effect was demonstrated via inexpensive and disposable plastic gratings on commercially available CDs and DVDs. Second, the effect of different line densities on the enhancement has been studied, and a peak output power of 3.6 mW was achieved under a loading resistance of 1 MΩ for the TENG with the aluminum
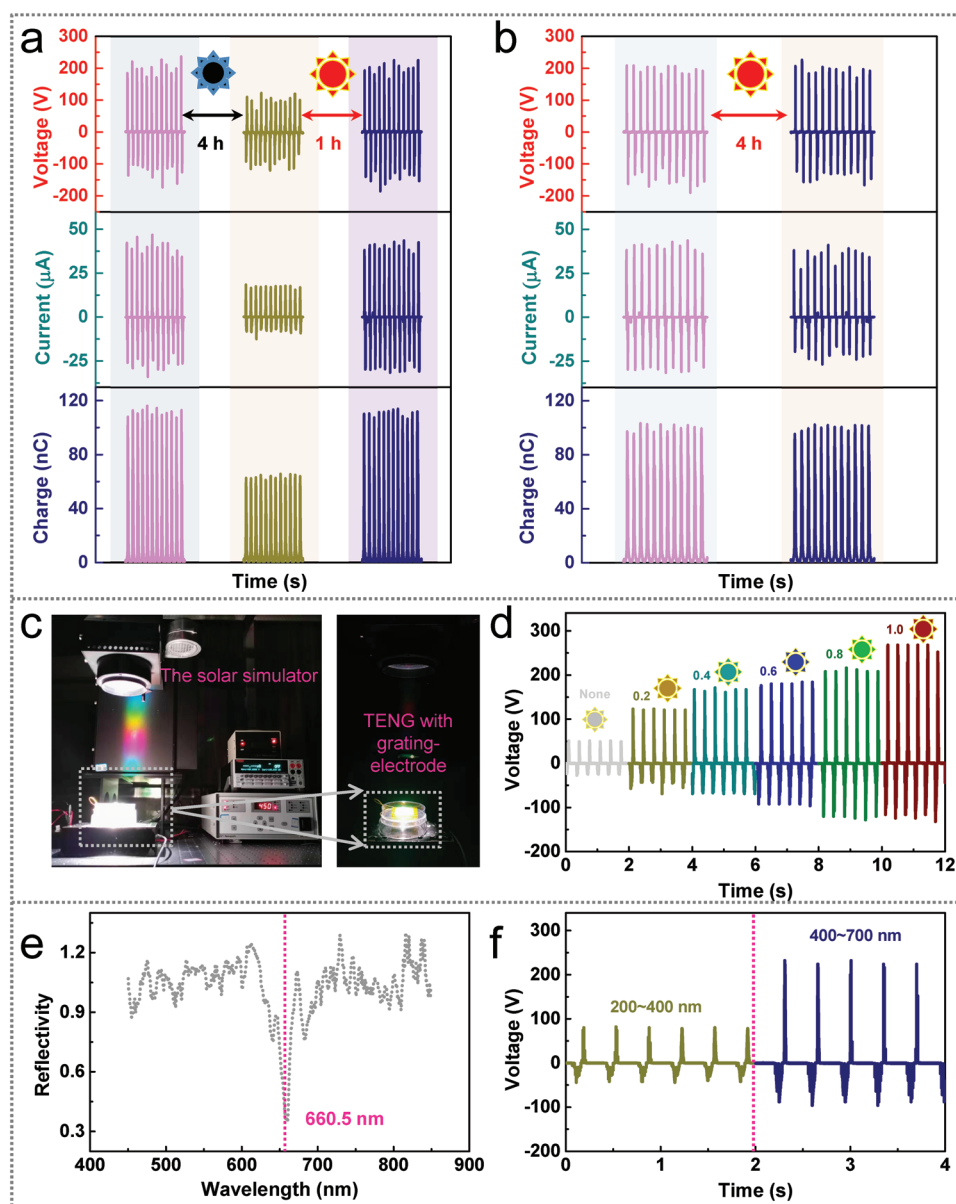
Figure 4. The effect of light intensity and wavelength on the output of TENG. a,b) The output performance of the TENG with the aluminum foil in the linear density of 600 after light and dark treatment. c) Lighting system. d) The effect of light intensity on the output of the TENG. e) The reflectivity curve of the grating electrode in 600 lines mm^{-1}. f) The output of TENG with the aluminum foil in the linear density of 600 lines mm^{-1} under 200–400 nm and 400–700 nm illuminating.

foil in the line density of 600 lines mm^{-1}, giving over 4.5-fold enhancement in output power (0.8 mW) and 75% reduction in output impedance compared with the TENG with the aluminum foil of no grating line. Furthermore, through light and dark treatment experiments, it was further verified that the enhancement was not due to the instantaneous effect of surface plasmon resonance, but the hot hole pairs effect. A systematical effect of the light intensity and wavelength on the output of TENG was also acquired. Finally, the capability of the TENG with the aluminum foil in the line density of 600 lines mm^{-1} in powering portable electrics has been demonstrated by a self-powered ultrasonic ranging system. Moreover, our findings may also give new insights into the improvement of output

characteristics of TENGs and accelerate their commercialization and applications.

4. Experimental Section

Fabrication of PDMS Films with Grating Bottom Electrode: PDMS films with grating bottom electrode were prepared successively by means of defoaming mixer (THINKY MIXER AR-100, THINKY), glue homogenizer (EasyCoater 4, Schwan technology), and vacuum drying oven (DZF-6030-T), and the detailed flow is shown in Figure S5a (Supporting Information). In detail, the PDMS elastomer and the curing agent (Sylgard 184, Dow Corning) were first thoroughly mixed in the weight ratio of 10:1 (Figure S5a (I), Supporting Information),
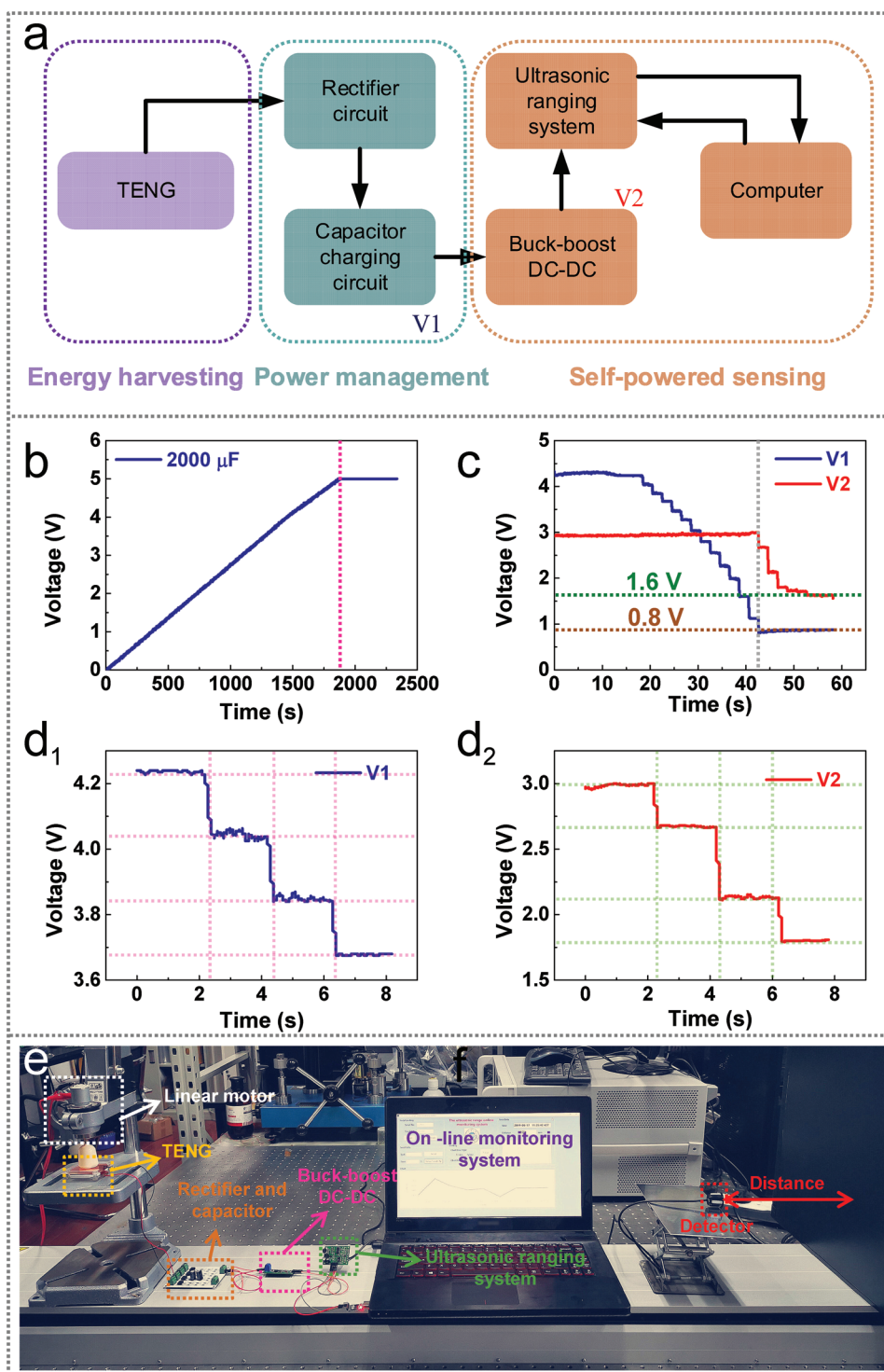
Figure 5. Power-supplying system to ultrasonic ranging system. a) Schematic diagram of a self-powered ultrasonic ranging system. b) The charging curve of TENG with the aluminum foil in the line density of 600 for a capacitor of 2000 μF. c) Output curves of capacitor (V1) and buck-boost DC–DC circuit (V2) in self-powered ultrasonic ranging system. d$_1$–d$_2$) The partial enlargements of V1 and V2. e) Photograph of a self-powered ultrasonic ranging system.

and then the mixture was thoroughly stirred by a mechanical blender for 5 min to obtain a uniform solution (Figure S5a (II), Supporting Information). After that, the mechanical blender was set as the defoaming mode for 2 min to remove the bubbles in the solution (Figure S5a (II), Supporting Information). Four pieces of aluminum foil with different line density gratings (0, 100, 300, 600 lines mm^{-1}) were then attached to the bottoms of four petri dishes in a flat manner, respectively (Figure S5a (III), Supporting Information).

1902725 (9 of 11)

Next, the solution was spin-coated onto the aluminum foil (act as the bottom electrode) at 300 RPM for 150 s. After all the solution was initially rotary coated on the aluminum foil, high-speed rotary coating (1000 RPM) was adopted for 30 s to make the mixed solution more even (Figure S5a (IV), Supporting Information). Then, the film was dried at 90 °C for 2.5 h in a hot vacuum oven (Figure S5a (V), Supporting Information). Finally, PDMS film attached with aluminum foils was peeling from the petri dish, whereupon thin PDMS film with grate-like aluminum foil base electrode was obtained as illustrate in Figure S5b (Supporting Information).

Fabrication of the TENG: The prepared films were cut into dimensions of 3.5 cm × 3.5 cm to fabricate TENGs. Figure S5c (Supporting Information) shows the double-layer TENG made of prepared film. The prepared films with dimensions of 3.5 cm × 3.5 cm were attached onto some pieces of PMMA (5 cm × 5 cm × 0.3 cm) as one triboelectric layer. The other triboelectric layers were some thin copper foils with the same dimensions of 3.5 cm × 3.5 cm attached onto another PMMA (5 cm × 5 cm × 0.3 cm). Then the two triboelectric layers were attached onto the linear motor and the support plate, respectively.

Construction of Ultrasonic Ranging System: The outputs of the TENG were connected to the power end of the ultrasonic ranging system successively after passing the rectifier bridge (DBS106), capacitor(2000 µF), and DC–DC circuit (LTC3106). Then the transmitted data were connected to a computer via a serial port for real-time monitoring.

Construction of Lighting System: The excitation was a solar simulator (Newport, 2612 A). Spectral curves were measured by a spectrometer (Ocean Optics USB 2000+). P-polarized light was generated by a linear polarizer (wp25m-vis).

Characterization: The outputs (voltage, short-circuit current, and transfer charge quantity) of the TENG (as depicted in Figures 2d,e, 3c–e, and 4a,b) were acquired by a programmable electrometer (Keithley model 6514) and a Data Acquisition Card (NI PCI-6259) on a Desktop PC, and the external excitation was provided by a linear motor (DIY-37GB330).The voltage data depicted in Figures 4d,e and 5b–d were acquired by an oscilloscope (mso2024B). The external excitation for Figure 4d,e was provided by a linear motor (DIY-O1-DC 3–6 V).

Supporting Information

Supporting Information is available from the Wiley Online Library or from the author.

Acknowledgements

Conflict of Interest

The authors declare no conflict of interest.

[1] Z. L. Wang, *Faraday Discuss.* **2014**, *176*, 447.
[2] Z. L. Wang, *ACS Nano* **2013**, *7*, 9533.
[3] J. S. Chun, B. U. Ye, J. W. Lee, D. Choi, C. Kang, S. Kim, Z. L. Wang, J. M. Baik, *Nat. Commun.* **2016**, *7*, 12985.
[4] S. H. Wang, X. J. Mu, Y. Yang, C. L. Sun, A. Y. D. Gu, Z. L. Wang, *Adv. Mater.* **2015**, *27*, 240.
[5] S. H. Wang, X. J. Mu, X. Wang, A. Y. Gu, Z. L. Wang, Y. Yang, *ACS Nano* **2015**, *9*, 9554.
[6] P. Bai, G. Zhu, Y. S. Zhou, S. H. Wang, J. S. Ma, G. Zhang, Z. L. Wang, *Nano Res.* **2014**, *7*, 990.
[7] L. X. Gao, D. L. Hu, M. K. Qi, J. Gong, H. Zhou, X. Chen, J. F. Chen, J. Cai, L. K. Wu, N. Hu, Y. Yang, X. J. Mu, *Nanoscale* **2018**, *10*, 19781.
[8] M. H. Lai, B. L. Du, H. Y. Guo, Y. Xi, H. K. Yang, C. G. Hu, J. Wang, Z. L. Wang, *ACS Appl. Mater. Interfaces* **2018**, *10*, 2158.
[9] R. Cao, T. Zhou, B. Wang, Y. Y. Yin, Z. Q. Yuan, C. J. Li, Z. L. Wang, *ACS Nano* **2017**, *11*, 8370.
[10] J. J. Yang, F. Yang, L. Zhao, W. Y. Shang, H. F. Qin, S. J. Wang, X. H. Jiang, G. Cheng, Z. L. Du, *Nano Energy* **2018**, *46*, 220.
[11] R. H. Zhu, W. Tang, C. Z. Gao, Y. Han, T. Li, X. Cao, Z. L. Wang, *Nano Energy* **2015**, *14*, 193.
[12] W. Tang, J. Q. Tian, Q. Zheng, L. Yan, J. X. Wang, Z. Li, Z. L. Wang, *ACS Nano* **2015**, *9*, 7867.
[13] S. H. Wang, L. Lin, Z. L. Wang, *Nano Lett.* **2012**, *12*, 6339.
[14] F. R. Fan, L. Lin, G. Zhu, W. Z. Wu, R. Zhang, Z. L. Wang, *Nano Lett.* **2012**, *12*, 3109.
[15] L. Lin, Y. N. Xie, S. H. Wang, W. Z. Wu, S. M. Niu, X. N. Wen, Z. L. Wang, *ACS Nano* **2013**, *7*, 8266.
[16] J. Chen, G. Zhu, W. Q. Yang, Q. S. Jing, P. Bai, Y. Yang, T. C. Hou, Z. L. Wang, *Adv. Mater.* **2013**, *25*, 6094.
[17] Z. H. Lin, G. Zhu, Y. S. Zhou, Y. Yang, P. Bai, J. Chen, Z. L. Wang, *Angew. Chem.* **2013**, *125*, 5169.
[18] Y. Yang, H. L. Zhang, J. Chen, S. M. Lee, T. C. Hou, Z. L. Wang, *Energy Environ. Sci.* **2013**, *6*, 1744.
[19] Y. N. Xie, S. H. Wang, L. Lin, Q. S. Jing, Z. H. Lin, S. M. Niu, Z. Y. Wu, Z. L. Wang, *ACS Nano* **2013**, *7*, 7119.
[20] Z. H. Lin, Y. Xie, Y. Yang, S. Wang, G. Zhu, Z. L. Wang, *ACS Nano* **2013**, *7*, 4554.
[21] J. A. Juárez-Moreno, A. Ávila-Ortega, A. I. Oliva, F. Avilés, J. V. Cauich-Rodríguez, *Appl. Surf. Sci.* **2015**, *349*, 763.
[22] K. Y. Lee, J. Chun, J. H. Lee, K. N. Kim, N. R. Kang, J. Y. Kim, M. H. Kim, K. S. Shin, M. K. Gupta, J. M. Baik, S. W. Kim, *Adv. Mater.* **2014**, *26*, 5037.
[23] X. M. He, X. J. Mu, Q. Wen, Z. Y. Wen, J. Yang, C. G. Hu, H. F. Shi, *Nano Res.* **2016**, *9*, 3714.
[24] J. Chen, H. Y. Guo, X. M. He, G. L. Liu, Y. Xi, H. F. Shi, C. G. Hu, *ACS Appl. Mater. Interfaces* **2016**, *8*, 736.
[25] X. N. Xia, J. Chen, H. Y. Guo, G. L. Liu, D. P. Wei, Y. Xi, X. Wang, C. G. Hu, *Nano Res.* **2017**, *10*, 320.
[26] H. S. Wang, C. K. Jeong, M. Seo, D. J. Joe, J. H. Han, J. Yoon, K. J. Lee, *Nano Energy* **2017**, *35*, 415.
[27] R. Zia, M. Selker, P. Catrysse, L. Mark, *J. Opt. Soc. Am. A* **2004**, *21*, 2442.
[28] J. Chon, C. Bullen, P. Zijlstra, M. Gu, *Adv. Funct. Mater.* **2007**, *17*, 875.

**ADVANCED
SCIENCE NEWS**

www.advancedsciencenews.com

**ADVANCED
ENERGY
MATERIALS**

www.advenergymat.de

[29] H. Baida, D. Mongin, D. Christofilos, G. Bachelier, A. Crut, P. Maioli, N. D. Fatti, F. Vallée, *Phys. Rev. Lett.* **2011**, *107*, 057402.

[30] S. Nootchanat, A. Pangdam, R. Ishikawa, K. Wongravee, K. Shinbo, K. Kato, F. Kaneko, S. Ekgasit, A. Baba, *Nanoscale* **2017**, *9*, 4963.

[31] B. K. Singh, A. C. Hillier, *Anal. Chem.* **2006**, *78*, 2009.

[32] M. W. Knight, H. Sobhani, P. Nordlander, N. J. Halas, *Science* **2011**, *332*, 702.

[33] C. César, *Nat. Photonics* **2014**, *8*, 95.

[34] H. Nakanishi, K. J. Bishop, B. Kowalczyk, A. Nitzan, E. A. Weiss, K. V. Tretiakov, M. M. Apodaca, R. Klajn, J. F. Stoddart, B. A. Grzybowski, *Nature* **2009**, *460*, 371.

[35] S. Mubeen, J. Lee, N. Singh, S. KräMer, G. D. Stucky, M. Moskovits, *Nat. Nanotechnol.* **2013**, *8*, 247.

[36] D. K. Davies, *J. Phys. D: Appl. Phys.* **1969**, *2*, 1533.

[37] J. Wang, C. S. Wu, Y. J. Dai, Z. H. Zhao, A. Wang, T. J. Zhang, Z. L. Wang, *Nat. Commun.* **2017**, *8*, 8.

[38] A. Smith, C. Wang, D. N. Guo, C. Sun, J. X. Huang. *Nat. Commun.* **2014**, *5*, 5517.